Tubular TiC fibre nanostructures as supercapacitor electrode materials with stable cycling life and wide-temperature performance

Xia, Xinhui; Zhang, Yongqi; Chao, Dongliang; Xiong, Qinqin; Fan, Zhanxi; Tong, Xili; Tu, Jiangping; Zhang, Hua; Fan, Hong Jin

2015

Xia, X., Zhang, Y., Chao, D., Xiong, Q., Fan, Z., Tong, X., et al.(2015). Tubular TiC fibre nanostructures as supercapacitor electrode materials with stable cycling life and wide-temperature performance. Energy & environmental science, 8(5), 1559-1568.

https://hdl.handle.net/10356/97767

https://doi.org/10.1039/C5EE00339C

Energy & Environmental Science

Accepted Manuscript

This article can be cited before page numbers have been issued, to do this please use: X. Xia, Y. Zhang, D. Chao, Q. Xiong, Z. Fan, X. Tong, J. Tu, H. Zhang and H. J. Fan, *Energy Environ. Sci.*, 2015, DOI:

ROYAL SOCIETY OF CHEMISTRY

www.rsc.org/ees

View Article Online
DOI: 10.1039/C5EE00339C

Tubular TiC Fibre Nanostructures as Supercapacitor Electrode Material with Stable Cycling Life and Wide-Temperature Performance

Xinhui Xia,[a,b] Yongqi Zhang,[a] Dongliang Chao,[a] Qinqin Xiong,[b] Zhanxi Fan,[c] Xili Tong,[d] Jiangping Tu,[b] Hua Zhang,[c] and Hong Jin Fan[a,*]

Received (in XXX, XXX) Xth XXXXXXXXX 20XX, Accepted Xth XXXXXXXXX 20XX
DOI: 10.1039/b000000x

Xinhui Xia and Yongqi Zhang contributed equally to this work.

ABSTRACT

Highly active electrode materials with judicious design in nanostructure are important for the construction of high-performance electrochemical energy storage devices. In this work, we have fabricated tubular TiC fibre cloth as an interesting type of stable supercapacitve materials. Hollow microfibres of TiC are synthesized by carbothermal treatment of commercial T-shirts cotton fibres. To demonstrate the rational of nanostructuring in energy storage, the hollow fibres are further covered by interwoven TiC nanotube branches, forming 3D tubular all-TiC hierarchical fibres with high electrical conductivity, high surface area, and high porosity. For energy storage functions, organic symmetric supercapacitors based on the hollow fibre-nanotube (HFNT) TiC cloth electrodes are assembled and thoroughly characterized. The TiC-based electrodes show very stable capacitance in long charge/discharge cycles and at different temperatures. In particular, the integrated TiC HFNT cloth electrodes show a reasonably high capacitance (185 F/g at 2 A/g), better cycling stability at high-rates (e.g., 97% retention at room temperature after 150,000 cycles, and 67% at −15 ^{o}C after 50,000 cycles) than other control electrodes (e.g., pure carbon fibre cloths). It is envisaged that these 3D tubular TiC fibres cloth is also useful for solar cells and electrocatalysis.

KEYWORDS: Metal carbides · Titanium carbide · Hollow fibres · Supercapacitor · Temperature effect

View Article Online
DOI: 10.1039/C5EE00339C

INTRODUCTION

Power sources for modern mobile devices are required to store large quantities of electrical charges in small volumes, and simultaneously able to deliver the charges rapidly. However, these two requirements cannot always be fulfilled by a single energy-storing device. In the past decades, supercapacitors have emerged and greatly advanced the development of electrochemical energy storage. It is well known that typical supercapacitors include electric double-layer capacitors (EDLCs) arising from ion adsorption,[1-3] and pseudocapacitors originating from surface Faradic redox reactions.[4-6] Whatever the type, electrode materials are the key components, which determine the whole performance of full devices. Recently, the research on developing advanced electrode materials have made encouraging achievements by exploring new materials or nanoscale surface modification.[7-12] Nowadays, research on new electrode materials such as transition metal carbides or nitrides has emerged, but still scanty, due to their good EDLCs properties, excellent mechanical and chemical stability, and high electrical conductivity.[1, 3]

Titanium carbide (TiC) is one of most promising transition metal carbides with fascinating physical properties such as excellent chemical and thermal stability, high hardness, outstanding oxidation and corrosion resistance, and low electrical resistivity.[13-15] These properties make TiC attractive for a wide range of applications in wear-resistant coatings, superconducting devices, chemical catalysis and electrochemical energy storage.[16-20] Currently, micro/nanosize TiC have been prepared based on carbon nanotubes (CNTs) confined reaction,[15, 21-23] carbon thermal reduction,[17, 24-27] and chemical vapor deposition.[28-30] All these methods use different carbon sources including CNTs, graphite, activated carbon, polymers, hydrocarbon gases, and biomaterials (such as bamboo and cotton). It has been demonstrated that the final morphology of TiC is highly related with the adopted carbon sources. Of these carbon sources, the cheap bio-templates, especially cotton fibre, are highly preferable for the construction of TiC electrodes. Up to now, although different types of TiC micro/nanostructures have been synthesized,[15, 23, 27, 29, 31] no results about integrated TiC electrodes have been reported, let alone their applications for electrochemical energy storage.

In order to achieve high performance of electrodes (e.g., higher capacitance, better cycling life, higher power/energy density), it is now widely accepted that a directional design/fabrication of the electrode materials is the prerequisite. Tailored electrode material with judicious

View Article Online
DOI: 10.1039/C5EE00339C

nanostructure can meet the critical requirements such as enhanced ion/electron conductivity, faster reaction kinetics and stronger mechanical stability.[32-40] An integrated electrode usually consists of conductive micron-scale backbone (usually both as the support and active materials) and secondary nanosized active materials grown on the former. This integrated electrode is beneficial to the power/energy output because of a hierarchical porous system with different pore diameters, high surface areas, high conductivity network structure, as well as their binder-free and additive-free characteristics.

In the present work, we fabricated TiC tubular fibers, both 1D hollow microfibres and hollow fibre with nanotube branches and demonstrate their outstanding supercapacitive properties. The TiC hollow fibre cloth was prepared directly from commercial cotton T-shirt which acts as both the carbon source and sacrificial template. The TiC hollow fibre cloth is made up of interconnected nanoparticles, and shows a high electrical conductivity (up to 10^5 S/m). To further push up the performance and demonstrate the rational of nanostructuring, secondary interwoven TiC nanotubes are grown onto the hollow fibre cloth skeleton to obtain integrated all TiC hollow fibre-nanotube (HFNT) electrodes. This integrated structure further improves the surface area and porosity. For preliminary demonstration, organic symmetric supercapacitors based on the tubular TiC fibre electrodes are assembled and thoroughly characterized. Remarkably, the symmetric supercapacitors based on the integrated HFNT electrodes exhibit noticeable high-rate capability and impressively stable cycling life at high rates (~97 % retention after 150,000 cycles at room temperature). Temperature-dependent (–15~65 ^{o}C) electrochemical properties are also conducted. Our study may stimulate attentions on a wide range of metal carbides in various nanostructures as high-performance electrode materials.

RESULTS AND DISCUSSION

View Article Online
DOI: 10.1039/C5EE00339C

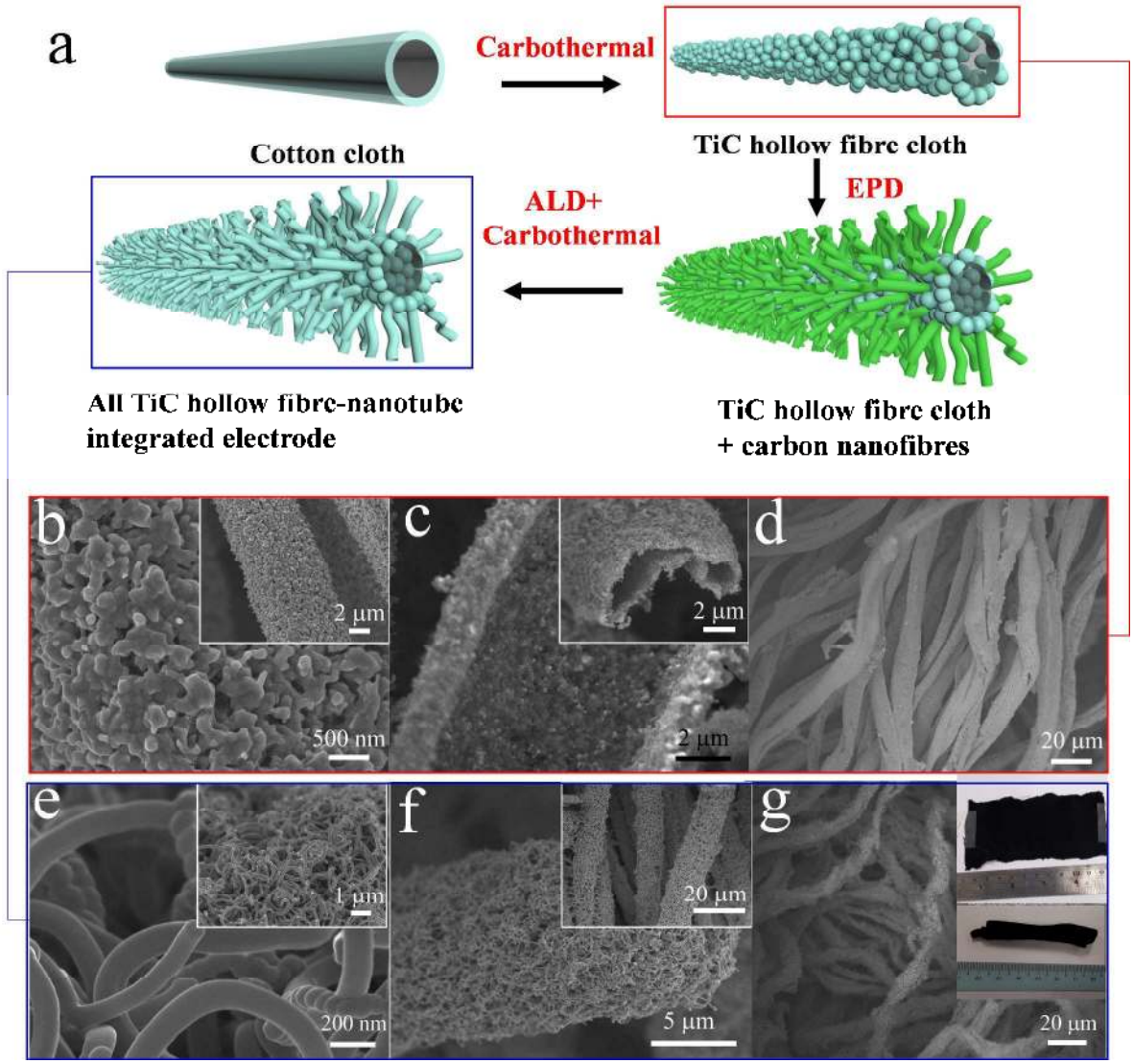

Figure 1 (a) Schematic of the fabrication process of TiC hollow fibre-nanotube (HFNT) integrated electrodes. (b-d) **SEM images of TiC hollow fibre cloth**: (b) Top view image (low-magnification SEM image in inset); (c) Cross-sectional image (hollow fibre structure in inset); (d) low-magnification view of the fiber bundles**. (e-g) SEM images of TiC hollow fibre-nanotube (HFNT) integrated electrodes**: (e) interwoven TiC nanotubes (low-magnification SEM image in inset); (f) TiC hollow fibre-nanotube composite fibre (low-magnification SEM image in inset); (g) low-magnification view (photos of TiC HFNT samples in inset).

Fabrication and characterization. Figure 1a shows the fabrication procedure of the integrated TiC HFNT electrodes prepared by the combination of carbothermal process, chemical vapor deposition (CVD), electrophoretic deposition (EPD) and atomic layer deposition (ALD)

View Article Online
DOI: 10.1039/C5EE00339C

technique. For the first step, the TiC hollow fibre cloth (HFC) is prepared by a facile carbothermal process using a commercial cotton T-shirt as both the carbon source and sacrificial template. Then, at the second step, CVD-derived carbon nanofibres are assembled on the surface of the TiC HFC via the EPD method. Finally, TiO_2 layer is coated on the surface of carbon nanofibres by ALD and then forms the integrated TiC HFNT electrodes after another carbothermal process. SEM images of cotton fibres are shown in Figure S1. The 100 % cotton T-shirt is composed of interconnected microscale hollow cotton fibres with diameters of 7–9 μm. Cotton has a striking hydrophilic ability that can absorb a large number of polar solvents such as water and ethanol. After soaking the cotton T-shirt in precursor solution for 24 h, the cotton T-shirt fully absorbs the solution with titanium source. After annealing at 1200 ^{o}C for 3 h in argon, the cotton cloth template is consumed and TiC hollow fibre cloth is successfully formed with well-preserved cloth morphology (Figure 1b-d and S2a, see experimental section). The obtained microscale TiC fibres (8–10 um) maintain the hollow structure (Figure 1c) and the walls of TiC fibres are made up of interconnected nanoparticles of 100–500 nm. Further insight into the microstructure of the TiC fibres is provided by TEM examination (Figure S2a and b). The TEM results confirm that the TiC fibre consist of interconnected nanoparticles of 100–500 nm leaving numerous nanopores of 10–100 nm. Moreover, the measured spacing between two adjacent lattice is 0.22 nm, which is consistent with the (002) planes of cubic TiC (JCPDS 65-0242). The phase and component of the TiC fibres are supported by XRD, Raman and energy dispersive (EDS) spectra analysis (Figure S2d-f). According to the BET test (inset in Figure S2e), the TiC hollow fibres exhibit a surface area of ~126 m^2/g.

In order to construct more porous electrode structures with higher surface areas, an intermediate step was taken to cover the TiC HFC with carbon nanofibres with diameters of 80–100 nm (Figure S3). Both sides of TiC fibre cloth undergo EPD to ensure uniform deposition of carbon nanofibres. The carbon nanofibres were pre-prepared by a standard CVD method (see the experimental section). The as-fabricated carbon nanofibres have two different morphologies: coiled fibres and common straight fibres. These two types of carbon nanofibres on the TiC hollow fibres are interwoven with each other forming a network of high surface area, rather than straight branches. More evidence of the amorphous carbon fibres are provided by XRD and Raman spectra (Figure S3g and h) as well as TEM examinations (Figure S4).

View Article Online
DOI: 10.1039/C5EE00339C

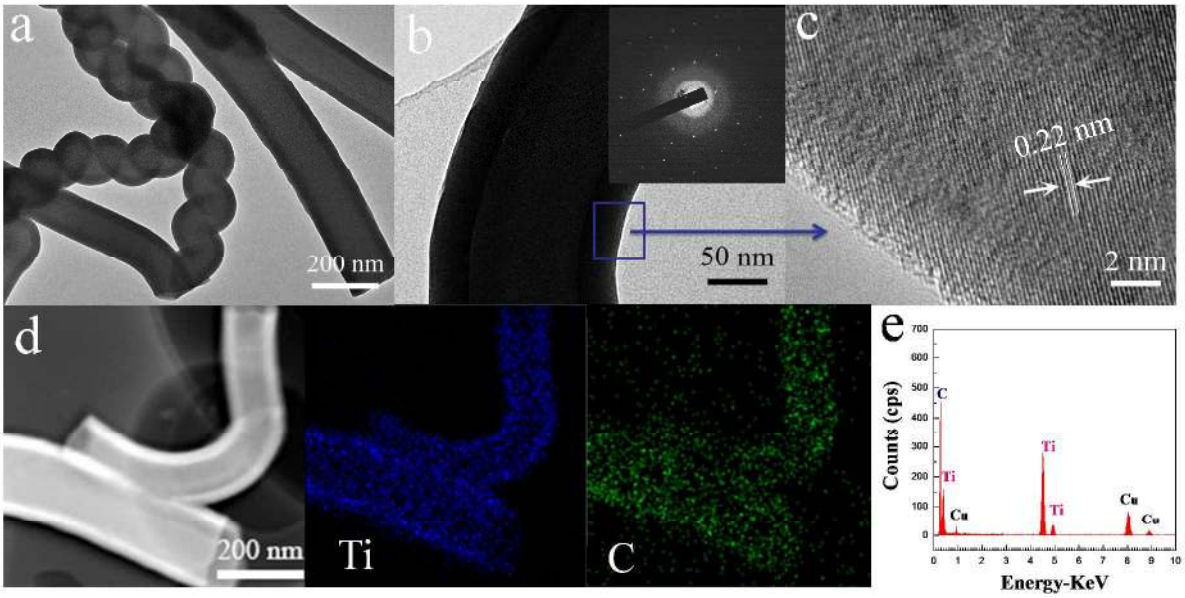

Figure 2 Characterization of TiC nanotubes. (a, c) TEM-HRTEM images (SAED pattern in inset). (d) Elemental maps of Ti and C of two TiC nanotubes. (e) EDS spectrum of TiC nanotubes.

The integrated TiC HFNT electrode is formed after another two steps: ALD and carbothermal treatment (Figure 1e-g). Here, the ALD-TiO_2 layer is first coated on the carbon nanofibres and finally converts into TiC nanotube after carbothermal treatment at 1200 ^{o}C for 3 h. The 3D porous architecture is well preserved for the integrated TiC HFNT electrodes, which consist of TiC hollow fibre substructure and TiC nanotube superstructure. Note that they are flexible like common cloth. The overall size of the branched fibre is about 12 μm (Figure 1e and f). The TiC nanotubes exhibit smooth surface and diameters ranging from 180 to 200 nm (Figure 1e). These nanotubes are also interwoven with each other. The tubular structure of TiC is clearly distinguished from the TEM images (Figure 2a-b). The wall thickness of the TiC nanotubes is about 50 nm, the same as ALD TiO_2 thickness. In addition, the SAED pattern reveals the existence of crystalline TiC and the lattice fringes with a lattice spacing of 0.22 nm corresponds to the (002) planes of cubic TiC (JCPDS 65-0242) (Figure 2c). The composition of the nanotube is further confirmed by the elemental maps of Ti and C (Figure 2e) and EDS spectrum (Cu is from the TEM copper grid) (Figure 2d).

View Article Online
DOI: 10.1039/C5EE00339C

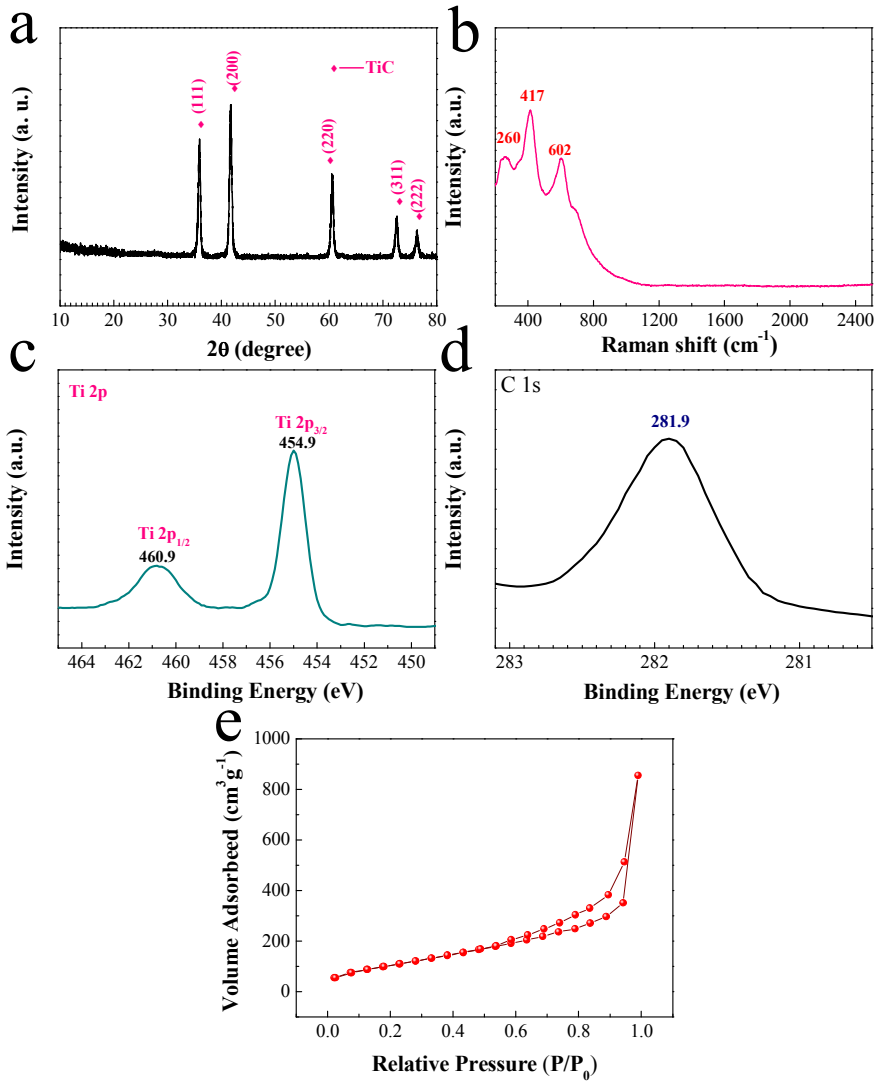

Figure 3 Structural and composition characterization of TiC HFNT electrodes: (a) XRD pattern; (b) Raman spectrum. XPS spectra: (c) Ti 2p spectrum and (d) C1s spectrum. (e) BET measurement-isothermal curve.

The integrated TiC HFNT electrodes are further characterized by XRD, Raman and XPS to check the phase and component. Data are presented in Figure 3. Compared with Figure S4a and b, the carbon peak disappears and only characteristic peaks of TiC are left in the XRD pattern and Raman spectrum (Figure 3a and b), confirming the TiC phase. Meanwhile, X-ray photoelectron spectroscopy (XPS) measurements were used to investigate the surface elemental

View Article Online
DOI: 10.1039/C5EE00339C

composition of the integrated TiC HFNT electrodes. For Ti 2p spectrum (Figure 3c), the observed binding energies of 454.9 and 460.9 eV are attributed to the Ti $2p_{3/2}$ and Ti $2p_{1/2}$ peaks of the TiC phase. The interval between two peaks is about 6.0 eV, which is in good agreement with that of TiC in the literature.[18-20] For C1s spectrum (Figure 3d), the broad peak at 281.9 eV is assigned to the carbon peak in a metal carbide environment. The specific surface area of the integrated TiC HFNT electrodes is calculated to be ~255 m^2/g (Figure 3e), which is higher than that (~126 m^2/g) of the TiC HFC electrodes above. More importantly, the integrated TiC HFNT electrodes have a high electrical conductivity up to ~1.1×10^5 S/m measured by four points probe technique. It is well accepted that high electrical conductivity and large surface area are of great importance for the higher performance in electrochemical energy storage devices (batteries and supercapacitors). For our TiC HFNT electrodes, we now see that all these desirable characteristics are integrated into one, thus superior electrochemical energy performance could be anticipated.

Supercapacitor performance. To demonstrate the potential application for electrochemical energy storage, in the present work, we assembled coin-type symmetric supercapacitors with the integrated TiC HFNT electrodes as both cathode and anode in organic electrolyte composed of 1.5 M $LiClO_4$ acetonitrile solution (see experimental section). It is noteworthy that our organic electrolyte has the advantages of high voltage window (0 – 2 V) and wide-temperature (-45 – 80 ^oC) stability compared to water electrolyte. Water electrolyte has a narrower voltage window of 0–1.23 V. And in water electrolyte, detrimental side reactions such as oxygen evolution reaction will occur, which is particularly serious as temperatures above 45 ^oC. For comparison, we also assembled symmetric supercapacitors based on other control electrodes: (i) Carbon fibre cloth electrode prepared from cotton T-shirt (designated as CFC, an electrical conductivity of ~1350 S/m) (Figure S5), (ii) Carbon fibre cloth supported carbon nanofibres electrode (designated as CFC+CNF, an electrical conductivity of ~1760 S/m) (Figure S6), and (iii) TiC hollow fibres cloth (designated as TiC HFC, an electrical conductivity of ~10^5 S/m). In our experiment, the selected working voltage window is 0–1.6 V, which is a very stale voltage window that side reactions such as decomposition of electrolyte can be avoided.

As shown by Figure 4a, b and S7, obviously, all four electrodes exhibit typical EDLC behavior with rectangular CV curves at different scanning rates and no redox peaks are observed.

View Article Online
DOI: 10.1039/C5EE00339C

This indicates that TiC is an active EDLC material similar to carbon, which is also supported by the CV at the low scanning rate (2.5 mV/s) and Raman measurement before and after charging (Figure S8). Comparatively, supercapacitors with the TiC HFNT electrodes show much higher current density and larger enclosed area of the CV curve than other counterparts at the same scanning rate (Figure S9a), implying their best electrochemical reactivity and energy storage performance, followed successively by TiC HFC, CFC+CNF and CFC electrodes. This result is supported by the corresponding charge/discharge measurements at 2A/g and 0.5 A/g (Figure S9b and c). Electrochemical impedance spectroscopy (EIS) test was conducted to elucidate the superior performance of the TiC HFNT electrodes. Figure 4c shows the Nyquist plots of all four electrodes at room temperature at the fully discharge state. The four plots all consist of a depressed semicircle in the high-frequency range and a long low-frequency line. The intercept on the Z real axis is attributed to the resistance of electrolyte (R_s), the diameter of semicircle reflects the charge transfer resistance (R_{ct}) related with the charge transfer through the electrode/electrolyte interface. Apparently, the TiC HFNT electrodes have the smallest of Rs value and amplitude of the semicircle, indicating their lowest charge transfer resistance and electrolyte resistance, followed successively by TiC HFC, CFC+CNF and CFC electrodes. Such integrated highly conductive network can enhance the charge transfer kinetics and diminish the polarization, resulting in high-rate performance.

The electrochemical results (specific capacitance at different rates, energy density and power density) of all four symmetric supercapacitors at the room temperature are shown in Figure 4d, S10 (also tabulated in Table S1 and S2). The TiC HFNT electrodes exhibit a specific capacity ranging from 185 F/g (41.6 F/cm^3) at 2A/g to 146 F/g (32.8 F/cm^3) at 30 A/g (based on the mass of one electrode). 79% capacitance is maintained when the current changes from 2 to 30 A/g. These values are higher than those of other counterparts. This capacitance improvement is also reflected in the full supercapacitors (see Figure S10b and Table S2). The full supercapacitors base on the TiC HFNT electrodes show a capacity of 44 F/g at 1A/g and 34.8 F/g at 15 A/g (based on the total mass of cathode, anode and separator), around 1.5 times higher than the counterparts with TiC HFC and CFC+CNT electrodes, and 2.8 times higher than the supercapacitors with CFC electrodes. Ragone plots in Figure 4e (also Table S2) shows the comparison of the power and energy densities of full supercapacitor devices. The all-TiC HFNT based supercapacitor shows an energy density of 12.4 Wh/kg at the power density of 11 kW/kg.

View Article Online
DOI: 10.1039/C5EE00339C

This value is higher than all rest three counterparts. These results demonstrate the noticeable high-rate capability and high energy/power performance of the TiC HFNT electrodes at room temperature (25 ^{o}C). Such outstanding performance of the TiC HFNT electrodes originates from the rational design of the hierarchical structure. *First*, the robust connection of microscale hollow fibre substructure and nanotube superstructure can efficiently provide large active surface area, which facilitates the ion/electron transportation and shortens their transfer path. *Second*, the good electrical conductivity of TiC decreases the charge transfer resistance resulting in lower inner resistance and better reaction kinetics. Both features account for the high-rate capability.

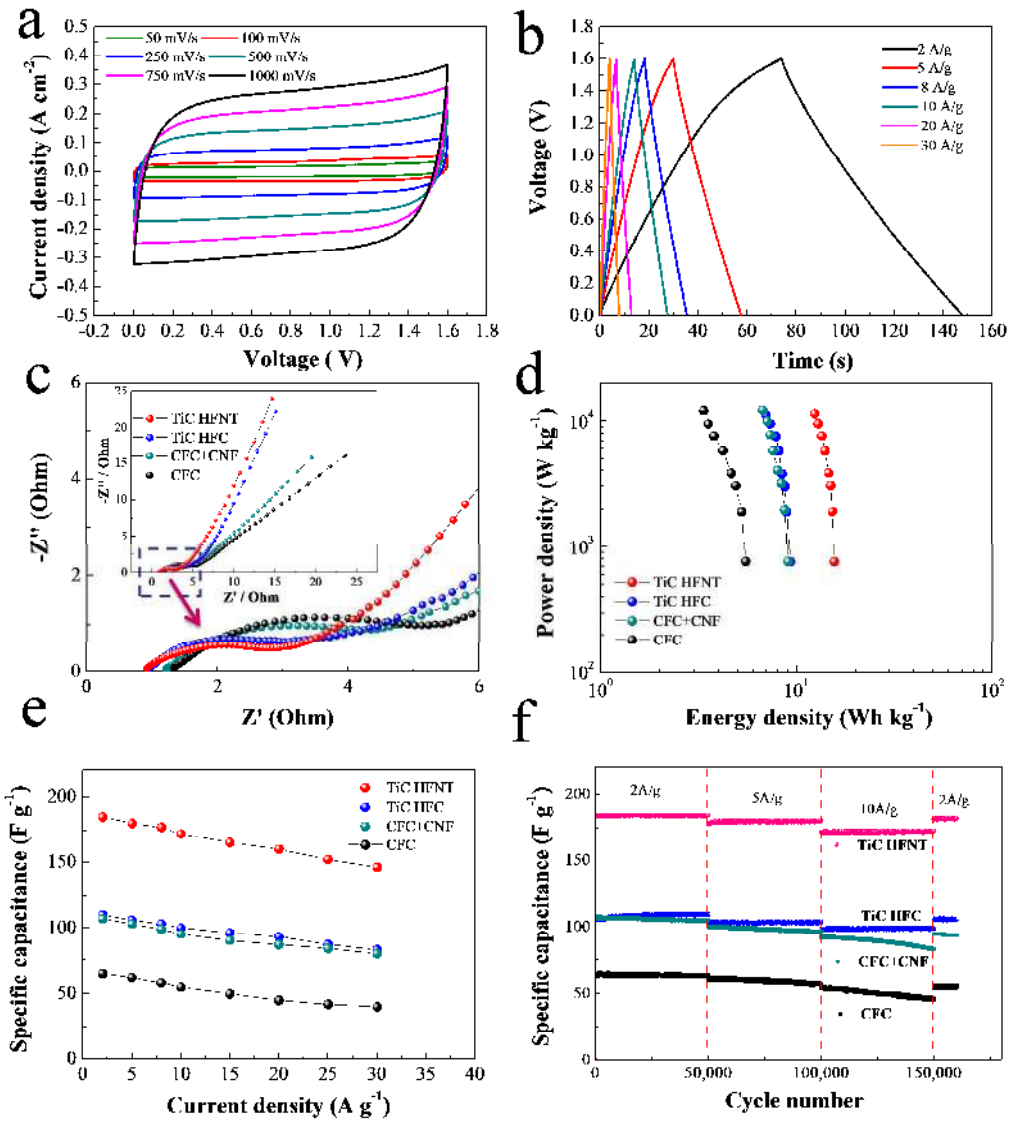

View Article Online
DOI: 10.1039/C5EE00339C

Figure 4 Electrochemical characterization of supercapacitors at room temperature (25 ^{o}C): (a) CV curves and (b) charge/discharge curves of the supercapacitor based on TiC HFNT electrodes. Data for supercapacitors made from other electrodes are presented in Figure S7. (c) Nyquist plots; (d) Specific capacitances of four electrodes; (e) Ragone plots of full supercapacitors; (f) Cycling performance of four electrodes at different current densities.

The full supercapacitor is very stable in cycling tests up to 160,000 cycles. Figure 4f shows the high-rate cycling trend of four supercapacitors at 25 ^{o}C (numerical data in Table S3). Impressively, the TiC HFNT electrodes exhibit excellent cycling life and deliver a high capacitance retention of 99 % at 2 A/g after 50,000 cycles (183 F/g), 98 % at 5A/g after 100,000 cycles (176 F/g), and 97 % at 10 A/g after 150,000 cycles (169 F/g), respectively. The excellent cycling stability can be ascribed to the structural stability of the electrode materials; no evident degradation of the hollow fibers or nanotubes was observed by SEM and TEM examinations after 160,000 cycles (see Figure S11). It is worth noting that both TiC-based electrodes (TiC HFNT and TiC HFC) have very stable cycling life compared to the carbon-based ones (CFC+CNF and CFC). Through a comprehensive comparison (see Table S4), the electrochemical results of the TiC HFNT electrodes are comparable, or superior to some carbon based materials,[41-45] but lower than some highly porous nanocarbons,[46-48] and the light-weight and highly-conductive 3D graphene/carbon nanotube composite electrodes.[49-51] It is known that carbon material electrodes may have the issue of oxidation under high current densities. The ability of anti-oxidation of the TiC electrodes is therefore advantageous for the operation at high current densities, leading to excellent rate capability. Therefore, it is indicated that the TiC-based electrodes are a promising type of EDLC electrode for high-performance supercapacitors.

View Article Online
DOI: 10.1039/C5EE00339C

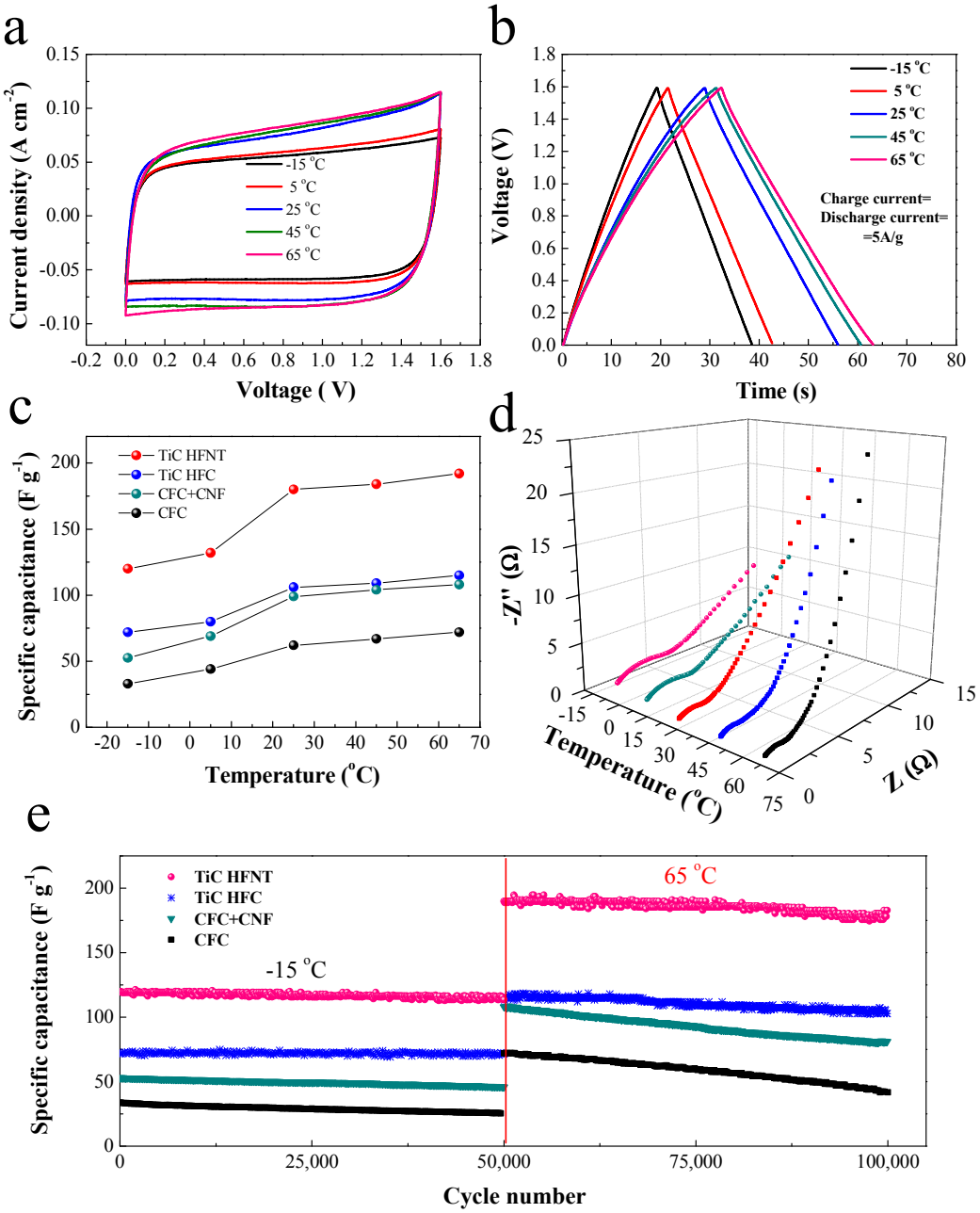

Figure 5 Electrochemical properties of the supercapacitors at different working temperatures. (a) CV curves (a scanning rate of 200 mV/s) and (b) charge/discharge curves of supercapacitors base on TiC HFNT (a current density of 5A/g). (c) Specific capacitances of four electrodes; (d) Nyquist plots of TiC HFNT electrodes; (e) Cycling life of four electrodes at a current density of 5 A/g.

View Article Online
DOI: 10.1039/C5EE00339C

We now present and discuss the temperature-dependent electrochemical property of the full supercapacitors. It is well known that the working temperature will greatly affect the ion conductivity and stability of the electrolyte. From the CV curves and galvanostatic charge/discharge profiles (Figure 5a, b and S12), it is clear that the reactivity and capacitance of all four electrodes increase with the working temperature from −15 to 65 ^{o}C. This phenomenon is due to the fact that the organic electrolyte has better ion conductivity at higher working temperatures (see EIS data below) and leads to higher capacitance and electrochemical reactivity. As shown in Table S5 and Figure 5c, the TiC HFNT electrodes deliver a capacitance of 120 F/g at −15 ^{o}C, which increases to 192 F/g at 65 ^{o}C (base on the mass of single electrode). And again the capacitance of the TiC HFNT electrode is consistently higher than other types of electrodes. Similar results are obtained in full supercapacitors. In particular, the capacitances of TiC-based electrodes (TiC HFNT and TiC HFC electrodes) at −15 ^{o}C account for ~67 % of the values obtained at 25 ^{o}C, much higher than the carbon-based electrodes (CFC+CNF and CFC electrodes, 53−54 %), implying that the TiC-based electrodes possess a high working efficiency at low temperatures and are good active materials for low-temperature supercapacitors. At high temperature of 65 ^{o}C, capacitance enhancement is observed for all electrodes and do not show degradation due to the temperature-stability of our organic electrolyte (no decomposition and side reactions up to 65 ^{o}C). To check the reactivity of electrode at different temperatures, EIS measurements of the TiC HFNT electrodes were conducted from −15 to 65 ^{o}C (Figure 5d). Note that both the resistance of electrolyte and the charge transfer resistance decreases with increasing the working temperature. The higher ion conductivity at higher temperatures corresponds to better reaction kinetics, in agreement with the abovementioned CV and charge/discharge results. The TiC-based electrodes also have an excellent cycling stability at both −15 ^{o}C and 65 ^{o}C for at least 50,000 cycles (Figure 5e and Table S6). In addition, at temperatures higher than 65 ^{o}C, the device performance starts to become worse, in particular the cycling performance. At higher temperatures, the electrolyte becomes more volatile, which may cause inner pressure of the full devices and lead to catastrophic impact on the electrode. This is more serious when the temperature is above 75 ^{o}C. Based on these electrochemical results above, we can confidently conclude that the TiC-based integrated electrodes possess superior wide-temperature supercapacitive performance (higher capacitance and better high-rate capability) and excellent long cycling life; Both are superior to the corresponding carbon-based counterparts.

View Article Online
DOI: 10.1039/C5EE00339C

CONCLUSIONS

We have directionally designed and fabricated TiC tubular fibre cloth as a new supercapacitor electrode material. The TiC electrodes are constructed from commercial cotton T-shirt as both carbon source and sacrificial template. In particularly, the all-TiC hollow fibre-nanotube integrated electrode shows high conductivity and interconnected porous structure. The organic symmetric supercapacitors based on TiC HFNT integrated electrodes show outstanding EDLC performance with relatively high capacitance and stable cycling life at both low and high temperatures. Therefore, the TiC hollow fibre electrodes could be a promising wide-temperature EDLC material with excellent anti-degradation in organic electrolyte. While the weight specific capacitance of the tubular TiC fibre cloth electrode is still not competitive to carbon nanotubes or graphene, it is comparable or even superior to many carbon materials (see Supporting Information). In all, we have demonstrated not only the potential of TiC for supercapacitors but also the rational of nanostructuring in boosting the energy storage performance.

EXPERIMENTAL

Preparation of TiC hollow fibre cloth (HFC) electrodes. In a typical synthesis, 0.3 g $Ni(NO_3)_2$ and 0.6 g NaF were first dissolved into 50 mL ethanol and then 1.8 g TiO_2 powder was added to form emulsion under ultrasound irradiation. After stirring for 2 h, a piece of cotton T-shirt with 5×10 cm^2 was dipped into the above emulsion and stirred for 3 h, then the cotton textile was taken out and dried at 110 ^oC for 2 h. Finally, the cotton textile was placed in a sealed corundum crucible and heated at 1200 ^oC for 3 h under continuous flow of argon. The carbothermal reactions for the formation of TiC fibres were very complex. The involved reactions might be as follows.[25]

$$NaF\ (l) \rightarrow Na\ (g) + F_2\ (g) \qquad (1)$$

$$Ni@C\ (s) \rightarrow Ni(C)\ (l) \qquad (2)$$

$$2TiO_2\ (s) + x\ F_2\ (g) + 4C\ (s) \rightarrow 2TiF_x\ (g) + 4CO \qquad (3)$$

$$2TiF_x\ (g) + 2Ni(C)\ (l) \rightarrow 2Ni(Ti, C)\ (l) + x\ F_2\ (g) \qquad (4)$$

$$Ni(Ti, C)\ (l) \rightarrow TiC\ (s) + Ni\ (l) \qquad (5)$$

View Article Online
DOI: 10.1039/C5EE00339C

After that, the sample was immersed in 0.2 M $KMnO_4$ for 1 h at 85 ^oC and 0.2 M HCl for 1 h, respectively, to remove the left carbon and nickel catalyst to obtain TiC hollow fibre cloth (HFC) electrodes.

Preparation of TiC hollow fibre-carbon nanofibre electrodes. First, carbon nanofibre powder was fabricated by a chemical vapor deposition (CVD) method. The catalyst precursor was prepared by mixing 50 ml of 0.1 M $CuCl_2$ and 50 ml of 0.1 M sodium–potassium tartrate to form copper tartrate precipitate. The dried copper tartrate was transferred to the reaction tube. The CVD reaction was conducted at 250 ^oC for 2 h in argon with flowing acetylene as the carbon source under atmospheric pressure. Then, the sample was immersed in solution of 1 M $FeCl_3$ and 0.5 M HCL for 3 h to completely dissolve the copper catalyst. Finally, the sample was annealed at 800 ^oC for 4 h under argon to form carbon nanofibres. The obtained carbon nanofibres were deposited on the surface of TiC hollow fibre cloth by an electrophoretic deposition (EPD) method. Electrolyte for EPD was obtained by dispersing 50 mg carbon nanofibre powder in 100 ml isopropyl alcohol to form stable carbon nanofibre colloids after adding 50 mg $Mg(NO_3)_2$. The EPD was performed in a standard two-electrode glass cell at room temperature, TiC hollow fibre cloth a size of 2×3 cm^2 as the working electrode and a Pt foil as the counter-electrode. The distance between the two electrodes was 1 cm and the EPD was carried out by applying 60 V for 80 s. Two sides of the TiC hollow fibre cloth were both undergone EPD to ensure the homogeneous deposition of carbon nanofibres.

Preparation of TiC hollow fibre-nanotube (HFNT) electrodes. The TiC HFNT electrodes were synthesized by the combination of atomic layer deposition (ALD) and carbothermal process. A layer of TiO_2 (thickness ~50 nm) was coated on the surface on the carbon nanofibres on TiC hollow fibre cloth by atomic layer deposition (ALD Beneq TFS 200) with $TiCl_4$ and H_2O as the Ti and O precursors, respectively. Then, the samples were annealed at 1200 ^oC under argon atmosphere for 3 h to form the TiC HFNT integrated electrodes. The simplified reactions would be $TiO_2 + 3C \rightarrow TiC + 2CO$.

Preparation of carbon fibre cloth (CFC) electrodes. The CFC electrodes were prepared by a pyrolysis of commercial cotton T-shirt, which was annealed at 800 ^oC for 2 h in argon. The mass of CFC electrode is about 4.0 mg/cm^2.

Preparation of carbon fibre cloth supported carbon nanofibres (CFC+CNF) electrodes. The CFC+CNF electrodes were prepared by EPD of carbon nanofibres on CFC. The EPD process was the same as that aforementioned. The mass of CFC+CNF electrode is about 5.8 mg/cm^2.

Characterization of integrated electrodes. The phase and microstructure of samples were characterized by X-ray diffraction (XRD, RIGAKU D/Max-2550 with Cu Kα radiation), field emission scanning electron microscopy (FESEM, FEI SIRION), high-resolution transmission electron microscopy (HRTEM, JEOL JEM-2010F), Raman spectroscopy (WITec-CRM200 Raman system with a laser wavelength of 532 nm), Fourier transform infrared (FTIR) spectroscopy (Perkin Elmer System 2000 FTIR interferometer) and X-ray photoelectron spectroscopy (XPS, PHI 5700). The surface areas of smples were determined by BET measurements using a NOVA-1000e surface area analyzer.

Supercapacitor fabrication and electrochemical measurements. The electrochemical performances of the TiC HFNT integrated electrodes were tested in CR2025 coin-type symmetric supercapacitors, in which the TiC HFNT electrodes were used as both the positive and negative electrodes without any

View Article Online
DOI: 10.1039/C5EE00339C

ancillary materials. The mass of TiC HFNT electrodes was about 9 mg/cm^2, in which TiC hollow fibres and TiC nanotube was 6.1 and 2.9 mg/cm^2, respectively. In our experiment, the different components were weighed by using an analytical balance with high measure resolution (0.01 mg). The electrolyte was an organic electrolyte with 1.5 M $LiClO_4$ in nonaqueous acetonitrile solution. The positive and negative electrodes were separated by a porous non-woven cloth separator and assembled into coin-type symmetric supercapacitors. A series of electrochemical measurements including cyclic voltammetry (CV) and electrochemical impedance spectroscopy (EIS) tests were performed on CHI660c electrochemical workstation (Chenhua, Shanghai). In order not to exceed the current range of electrochemical working station, the CV test was conducted using small-size (~0.5 cm^2) full supercapacitor devices. The EIS measurements were conducted with a superimposed 5 mV sinusoidal voltage in the frequency range of 100 kHz–0.01Hz. The galvanostatic charge/discharge test were conducted by Xinwei battery program-control test system with current range up to 10 A.

The specific capacitance and energy/power density were calculated as the following equations. For a symmetrical capacitor, assuming the capacitance of single electrode was C_S, then the total capacitance (C_T) of full supercapacitor would be ½ C_s according to the equation:

$$\frac{1}{C_T}=\frac{1}{C_S}+\frac{1}{C_S} \qquad (6)$$

The specific capacitance of full supercapacitor (C_{ST}) was calculated as the following equation.

$$C_{ST}=\frac{I\,\Delta t}{M\Delta V} \qquad (7)$$

where C_{ST} (F/g) was the specific capacitance of full supercapacitor, I (mA) represented discharge current through the full supercapacitors, and M (mg), ΔV (V) and Δt (s) designated the mass of full supercapacitors (here mainly including anode, cathode and separator), potential drop during discharge and total discharge time, respectively. The specific capacitance of full supercapacitors (C_{ST}) was about 4 Cs_T. The specific capacitance of single electrode (C_{SS}) was calculated as the following equation.

$$C_{SS}=\frac{2I\,\Delta t}{m\Delta V} \qquad (8)$$

where C_{SS} (F/g) was the specific capacitance of single electrode, I (mA) represented discharge current through the full supercapacitors, and m (mg), ΔV (V) and Δt (s) designated the mass of single electrode, potential drop during discharge and total discharge time, respectively.

Energy density (E_T) of the full supercapacitors was derived according to the following equation:

$$E_T=\frac{1}{2}C_{ST}\Delta V^2 \qquad (9)$$

Where E (Wh/kg) was the energy density, C_{ST} (F/g) was the specific capacitance of the full supercapacitors, and ΔV (V) was the discharge voltage range.

Power density (P) of the full supercapacitors was calculated from the following equation.

View Article Online
DOI: 10.1039/C5EE00339C

$$P = \frac{E_T}{\Delta t} \qquad (10)$$

where P (W/kg) was the power density, and Δt (s) was the discharge time .

Acknowledgements.

This work is supported by SERC Public Sector Research Funding (Grant number 1121202012), Agency for Science, Technology, and Research (A*STAR), and MOE AcRF Tier 1 (RG104/14). H. Z. acknowledges the support by Singapore MOE under AcRF Tier 2 (ARC 26/13, No. MOE2013-T2-1-034), AcRF Tier 1 (RG 61/12). This research is also funded by the Singapore National Research Foundation and the publication is supported under the Campus for Research Excellence And Technological Enterprise (CREATE) programme (Nanomaterials for Energy and Water Management). J. Tu acknowledgements the support by the Program for Innovative Research Team in University of Ministry of Education of China (IRT13037) and Key Science and Technology Innovation Team of Zhejiang Province (2010R50013). This work is also supported by the Foundation of State Key Laboratory of Coal Conversion (Grant No. J14-15-909).

Notes and references

[a] *Division of Physics and Applied Physics, School of Physical and Mathematical Sciences, Nanyang Technological University, Singapore 637371, Singapore*
email: fanhj@ntu.edu.sg
[b] *School State Key Laboratory of Silicon Materials, Key Laboratory of Advanced Materials and Applications for Batteries of Zhejiang Province, and Department of Materials Science and Engineering, Zhejiang University, Hangzhou 310027, China*
[c] *School of Materials Science & Engineering, Nanyang Technological University, Singapore 639798, Singapore*
[d] *State Key Laboratory of Coal Conversion, Institute of Coal Chemistry, Chinese Academy of Science, Taiyuan 030001, P. R. China*

† Electronic Supplementary Information (ESI) available. See DOI: 10.1039/b000000x/

1. C. Liu, F. Li, L. P. Ma and H. M. Cheng, *Adv. Mater.* , 2010, 22, E28-E62.

2. P. Simon and Y. Gogotsi, *Nat. Mater.*, 2008, 7, 845-854.

3. G. P. Wang, L. Zhang and J. J. Zhang, *Chem. Soc. Rev.*, 2012, 41, 797-828.

4. V. Augustyn, P. Simon and B. Dunn, *Energy Environ. Sci.*, 2014, 7, 1597-1614.

View Article Online
DOI: 10.1039/C5EE00339C

5. X. Xia, Y. Zhang, D. Chao, C. Guan, Y. Zhang, L. Li, X. Ge, I. M. Bacho, J. Tu and H. J. Fan, *Nanoscale*, 2014, 6, 5008-5048.

6. R. S. Devan, R. A. Patil, J.-H. Lin and Y.-R. Ma, *Adv. Funct. Mater.*, 2012, 22, 3326-3370.

7. J. T. Zhang, J. W. Jiang, H. L. Li and X. S. Zhao, *Energy Environ. Sci.*, 2011, 4, 4009-4015.

8. Y. Zhang, H. Feng, X. B. Wu, L. Z. Wang, A. Q. Zhang, T. C. Xia, H. C. Dong, X. F. Li and L. S. Zhang, *Int. J. Hydrogen Energy*, 2009, 34, 4889-4899.

9. F. Wang, S. Xiao, Y. Hou, C. Hu, L. Liu and Y. Wu, *RSC Adv.* , 2013, 3, 13059-13084.

10. Q. Zhang, E. Uchaker, S. L. Candelaria and G. Cao, *Chem. Soc. Rev.*, 2013, 42, 3127-3171.

11. X. Huang, Z. Y. Yin, S. X. Wu, X. Y. Qi, Q. Y. He, Q. C. Zhang, Q. Y. Yan, F. Boey and H. Zhang, *Small*, 2011, 7, 1876-1902.

12. X. Huang, Z. Y. Zeng, Z. X. Fan, J. Q. Liu and H. Zhang, *Adv. Mater.* , 2012, 24, 5979-6004.

13. V. Ern and Switendi.Ac, *Physical Review*, 1965, 137, A1927.

14. Y. Yao, K. F. Huo, L. B. Hu, N. A. Liu, J. J. Ha, M. T. McDowell, P. K. Chu and Y. Cui, *ACS Nano*, 2011, 5, 8346-8351.

15. H. J. Dai, E. W. Wong, Y. Z. Lu, S. S. Fan and C. M. Lieber, *Nature*, 1995, 375, 769-772.

16. Y. Gao, V. Presser, L. F. Zhang, J. J. Niu, J. K. McDonough, C. R. Perez, H. B. Lin, H. Fong and Y. Gogotsi, *J. Power Sources*, 2012, 201, 368-375.

17. X. Y. Tao, J. Du, Y. P. Li, Y. C. Yang, Z. Fan, Y. P. Gan, H. Huang, W. K. Zhang, L. X. Dong and X. D. Li, *Adv. Energy Mater.*, 2011, 1, 534-539.

18. Y. Cheng and Y. F. Zheng, *Surf. Coat. Technol.*, 2007, 201, 4909-4912.

19. A. Ignaszak, C. J. Song, W. M. Zhu, J. J. Zhang, A. Bauer, R. Baker, V. Neburchilov, S. Y. Ye and S. Campbell, *Electrochim. Acta*, 2012, 69, 397-405.

20. M. M. O. Thotiyl, S. A. Freunberger, Z. Q. Peng, Y. H. Chen, Z. Liu and P. G. Bruce, *Nat. Mater.*, 2013, 12, 1049-1055.

21. T. Taguchi, H. Yamamoto and S. I. Shamoto, *J. Phys. Chem. C*, 2007, 111, 18888-18891.

22. E. W. Wong, B. W. Maynor, L. D. Burns and C. M. Lieber, *Chem. Mater.*, 1996, 8, 2041-2046.

23. Y. Zhang, T. Ichihashi, E. Landree, F. Nihey and S. Iijima, *Science*, 1999, 285, 1719-1722.

24. N. Ahlen, M. Johnsson and M. Nygren, *J. Am. Ceram. Soc.*, 1996, 79, 2803-2808.

25. K. F. Huo, Y. M. Hu, Y. W. Ma, Y. N. Lu, Z. Hu and Y. Chen, *Nanotechnology*, 2007, 18.

26. H. L. Jia, Z. H. Zhang, Z. Qi, G. D. Liu and X. F. Bian, *J. Alloys Compd.*, 2009, 472, 97-103.

View Article Online
DOI: 10.1039/C5EE00339C

27. X. Y. Tao, Y. P. Li, J. Du, Y. Xia, Y. C. Yang, H. Huang, Y. P. Gan, W. K. Zhang and X. D. Li, *J. Mater. Chem.*, 2011, 21, 9095-9102.

28. C. H. Liang, G. W. Meng, W. Chen, Y. W. Wang and L. D. Zhang, *J. Cryst. Growth*, 2000, 220, 296-300.

29. S. R. Qi, X. T. Huang, Z. W. Gan, X. X. Ding and Y. Cheng, *J. Cryst. Growth*, 2000, 219, 485-488.

30. Y. W. Yuan and J. S. Pan, *J. Cryst. Growth*, 1998, 193, 585-591.

31. X. Y. Tao, J. Du, Y. C. Yang, Y. P. Li, Y. Xia, Y. P. Gan, H. Huang, W. K. Zhang and X. D. Li, *Cryst. Growth Des.*, 2011, 11, 4422-4426.

32. X. Cao, Y. Shi, W. Shi, G. Lu, X. Huang, Q. Yan, Q. Zhang and H. Zhang, *Small*, 2011, 7, 3163-3168.

33. C. Yuan, J. Li, L. Hou, X. Zhang, L. Shen and X. W. D. Lou, *Adv. Funct. Mater.*, 2012, 22, 4592-4597.

34. J. Ji, L. L. Zhang, H. Ji, Y. Li, X. Zhao, X. Bai, X. Fan, F. Zhang and R. S. Ruoff, *ACS Nano*, 2013, 7, 6237-6243.

35. L. L. Peng, X. Peng, B. R. Liu, C. Z. Wu, Y. Xie and G. H. Yu, *Nano Lett.*, 2013, 13, 2151-2157.

36. Z. Yan, L. Ma, Y. Zhu, I. Lahiri, M. G. Hahm, Z. Liu, S. Yang, C. Xiang, W. Lu, Z. Peng, Z. Sun, C. Kittrell, J. Lou, W. Choi, P. M. Ajayan and J. M. Tour, *ACS Nano*, 2012, 7, 58-64.

37. X. Yu, B. Lu and Z. Xu, *Adv. Mater.* , 2014, 26, 1044-1051.

38. X. Xia, D. Chao, Z. Fan, C. Guan, X. Cao, H. Zhang and H. J. Fan, *Nano Lett.*, 2014, 14, 1651-1658.

39. X. Xia, D. Chao, C. F. Ng, J. Lin, Z. Fan, H. Zhang, Z. X. Shen and H. J. Fan, *Mater. Horiz.*, 2015, 2, 237-244.

40. X. Xia, Y. Zhang, Z. Fan, D. Chao, Q. Xiong, J. Tu, H. Zhang and H. J. Fan, *Adv. Energy Mater.*, 2014, 1401709.

41. L. Demarconnay, E. Raymundo-Pinero and F. Béguin, *Electrochem. Commun.*, 2010, 12, 1275-1278.

42. D. Hulicova‐Jurcakova, M. Seredych, G. Q. Lu and T. J. Bandosz, *Adv. Funct. Mater.*, 2009, 19, 438-447.

43. C. Liu, Z. Yu, D. Neff, A. Zhamu and B. Z. Jang, *Nano Lett.*, 2010, 10, 4863-4868.

44. M. D. Stoller, S. Park, Y. Zhu, J. An and R. S. Ruoff, *Nano Lett.*, 2008, 8, 3498-3502.

45. Y. Wang, J. Chen, J. Cao, Y. Liu, Y. Zhou, J.-H. Ouyang and D. Jia, *J. Power Sources*, 2014, 271, 269-277.

View Article Online
DOI: 10.1039/C5EE00339C

46. J. R. McDonough, J. W. Choi, Y. Yang, F. La Mantia, Y. Zhang and Y. Cui, *Appl. Phys. Lett.*, 2009, 95, 243109.

47. E. Raymundo‐Piñero, F. Leroux and F. Béguin, *Adv. Mater.* , 2006, 18, 1877-1882.

48. Y. Liang, X. Feng, L. Zhi, U. Kolb and K. Müllen, *Chem. Commun.*, 2009, 7, 809-811.

49. Z. Fan, J. Yan, L. Zhi, Q. Zhang, T. Wei, J. Feng, M. Zhang, W. Qian and F. Wei, *Adv. Mater.* , 2010, 22, 3723-3728.

50. J. Hu, Z. Kang, F. Li and X. Huang, *Carbon*, 2014, 67, 221-229.

51. S. Ye, J. Feng and P. Wu, *ACS Appl. Mat. Interfaces*, 2013, 5, 7122-7129.

View Article Online
DOI: 10.1039/C5EE00339C

TABLE OF CONTENT

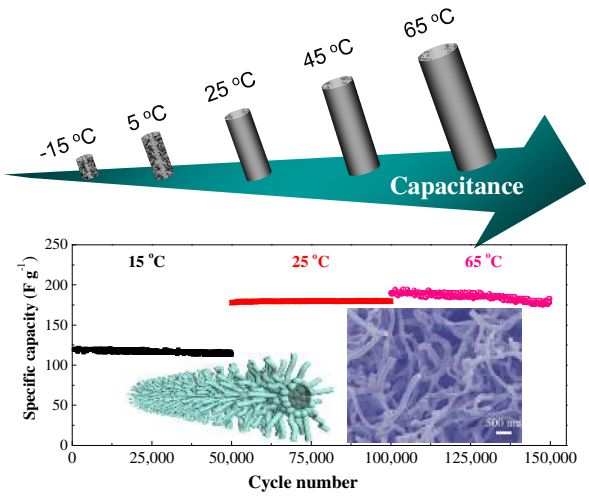

Hierarchical TiC hollow microfibres with nanotube branches are synthesized by carbothermal treatment of commercial T-shirts cotton fibres and thermal reaction of carbon nanofibre with ALD TiO_2. The branched TiC fibers demonstrate high-rate supercapacitor energy storage with remarkable wide-temperature specific capacitance and excellent cycling stability.